



Physikalisch-Technische Bundesanstalt  
National Metrology Institute

The following article is hosted by PTB;

DOI: 10.7795/EMPIR.19ENV02.PA.20231027 It is provided for personal use only.

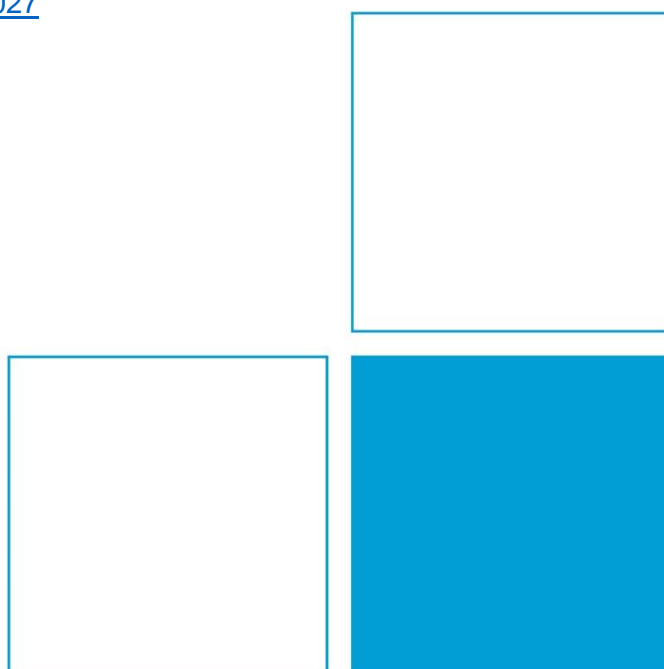
## A calibration methodology for the novel radioluminescence detector systems

**Faton S. Krasniqi, Richard Dieter Taubert, Stefan Röttger, Maksym Luchkov, Florian Mertes, Anja Honig, Christoph Baltruschat, Volker Dangendorf, Ulrich Giesen**

**Acknowledgement:** The project 19ENV02 RemoteALPHA has received funding from the EMPIR programme co-financed by the Participating States and from the European Union's Horizon 2020 research and innovation programme. 19ENV02 RemoteALPHA denotes the EMPIR project reference.

Available at:

<https://doi.org/10.7795/EMPIR.19ENV02.PA.20231027>



---

# A CALIBRATION METHODOLOGY FOR THE NOVEL RADIOLUMINESCENCE DETECTOR SYSTEMS

---

A PREPRINT

**F. S. Krasniqi\*, R. D. Taubert, S. Röttger, M. Luchkov, F. Mertes, A. Honig, C. Baltruschat, V. Dangendorf, and U. Giesen**

Physikalisch-Technische Bundesanstalt (PTB), Bundesallee 100, 38116 Braunschweig, Germany

October 26, 2023

## ABSTRACT

Radioluminescence mapping using well-characterized and optimized optical systems is an effective method for localizing contaminations with alpha-emitting radionuclides. To apply this novel approach to radiological emergency management, nuclear safeguards, nuclear decommissioning, and nuclear forensics, an established traceability chain is required. Within the EMPIR project 19ENV02 RemoteALPHA, SI-traceable calibration standards and procedures have been developed to provide the metrological basis for optical detection of alpha-emitting radionuclides. This work presents the development and implementation of a novel calibration methodology to provide valuable information about, and confidence in, the performance of radioluminescence detection systems. The proposed calibration methodology is based on two complementary approaches: (a) application of well-characterized activity standards to establish a traceable relationship between radioluminescence intensity and alpha activity, and (b) use of all-optical radiation-based devices that, when calibrated against an alpha activity standard, simulate the radioluminescence induced in nitrogen (N<sub>2</sub>) and nitric oxide (NO) gases by alpha particles in specific spectral regions. A dedicated <sup>210</sup>Po alpha activity standard with a sharp peak of less than 32 keV FWHM at 5.3 MeV and a surface activity of 648 kBq has been developed and used to characterize a lens-based radioluminescence detection system in terms of its sensitivity to alpha-induced radioluminescence in different atmospheres (air, N<sub>2</sub>, N<sub>2</sub> + NO mixture) in the UV-A and UV-C (solar blind) spectral regions. This detection system was used as an intermediary transfer device to cross-calibrate two portable integrating sphere-based radiance standards designed to simulate radioluminescence in the UV-A and UV-C spectral regions. The UV-A radiance standard simulates alpha source activities from  $3.6 \times 10^4$  Bq to  $5.1 \times 10^8$  Bq (340 nm central wavelength, 12 nm bandwidth), whereas the UV-C one from  $4.4 \times 10^5$  Bq to  $8.7 \times 10^4$  Bq (260 nm central wavelength, 16 nm bandwidth). These radiance standards substantially simplify routine quality control of radioluminescence detection systems by eliminating the need for open alpha sources, which are always associated with strict radiation safety precautions. Furthermore, since their intensity is adjustable over a very wide range, linearity and detection limits of radioluminescence detectors can be readily determined. The design, construction, radiometric characterization, and calibration of dedicated transfer standards, as well as the development of new calibration procedures for radiometric traceability of radioluminescence detection systems, will enable appropriate accident and post-accident radiation measurements that will lead to more effective countermeasures and better protection of people, wildlife, and the environment.

**Keywords** Alpha particles · Optical detection · Radioluminescence · Activity standard · Radiance standard · Emergency management

---

\*Corresponding author: faton.krasniqi@ptb.de

## 1 Introduction

Radioluminescent light is produced during the propagation of ionizing particles through a surrounding medium. In air, radioluminescence is generated mostly by emission of molecular nitrogen ( $N_2$ ) and nitrogen ions  $N_2^+$ , and to a much lesser extent, by trace amounts of nitric oxide (NO). The wavelength of radioluminescent light spans three ultraviolet (UV) bands (UV-A, UV-B, and UV-C), with about 95% of emission occurring in the 280 nm to 440 nm spectral range [1–3]. This process, discovered in the early years of the 20th century [4–6], was extensively studied by astrophysicists to determine the energy deposition and distribution of extended air showers [7–9]. The extensive knowledge gained in this process provided a solid basis for radioluminescence studies involving alpha particles, contributing to the development of new approaches that benefit nuclear safety, security, safeguards and radiological emergency management [2, 10, 11].

Effective detection of alpha contamination is a challenge for emergency management and for controlling nuclear safety because conventional measurement techniques require direct interaction of the alpha particles with the detector material, limiting the range of their detection to a few centimeters in air. Therefore, conventional detectors for alpha contamination, such as those based on scintillation technology (e.g., silver-activated ZnS films [12]) or semiconductor devices (e.g., passivated implanted planar silicon and silicon gold surface barrier detectors [13, 14]), must be positioned within a few centimeters of the source (typically within 4 cm) in order to detect alpha emissions. This causes significant drawbacks to the overall emergency management process, such as potential exposure of operators to other hazards and risks (e.g., other types of radiation, fire, etc.), potential contamination of detectors, long screening times, etc. These limitations can be overcome by using the radioluminescent light that alpha particles produce in air: UV light propagates in air over considerable distances, often kilometers, which exceeds the limited range of alpha particles in air (a few centimeters) by several orders of magnitude. This enables non-contact detection of contamination from a safe distance, reducing risks to personnel, reducing detection time, and minimizing costs.

The challenges, however, for the optical detection of alpha particles are still significant. First, most of the excitations in the air caused by alpha particles do not decay by radiation. Instead, the excitation energy is transferred to rotation, vibration or translation of other molecules without emitting optical photons [7]. This so-called, quenching effect limits the radioluminescence efficiency substantially making air a very poor scintillator. Second, the spectrum of radioluminescent light falls within the wavelength range of solar radiation and is outshone by it at wavelengths above 280 nm [1, 2]. At wavelengths shorter than 280 nm (the so-called solar-blind spectral region), on the other hand, the background light is very weak, in particular with daylight, because most of solar radiation is absorbed by the atmospheric ozone [2, 15]; The intensity of UV-C radioluminescence with wavelengths between 200 nm and 280 nm, however, is very low (<5%). Thus, both cases impose strict limitations on the wide application of this technique.

The EMPIR project 19ENV02 RemoteALPHA has developed several radioluminescence detection systems capable of efficiently detecting the weak radioluminescence of air in the UV-A and UV-C spectral regions, while being as insensitive as possible to ambient light [16, 17]. To facilitate the deployment of these systems for the management of radiological emergencies, nuclear safety, security and safeguards, SI traceable calibration schemes and standards have also been developed. The developed calibration schemes are source-based and rely on two complementary approaches. The first calibration method comprises the application of dedicated activity standards and environmental samples with deposited alpha source emitters, whereas the second method uses two purely optical radiation-based devices which simulate the radioluminescence in air induced by an alpha emitting source. In this paper, a UV Fused Silica (UVFS) lens-based radioluminescence detection system (reference instrument) has been characterized with the dedicated  $^{210}\text{Po}$  activity standard to provide the metrological basis for the optical detection of alpha-emitting radionuclides. Featuring high specific activity of  $1.66 \times 10^{14} \text{ Bq g}^{-1}$  and a sharp alpha peak at 5.3 MeV, the  $^{210}\text{Po}$  source has nearly ideal properties for traceable calibration of radioluminescence detector systems in terms of count rate per Becquerel and for determining the relationships between radiometric quantities and alpha activity. The UVFS lens-based reference instrument has been further used to cross-calibrate a UV-A and UV-C low-photon flux radiance standards that simulate the radioluminescence induced in air by an alpha-emitting sample of a circular shape with a diameter of 25 mm. Both radiance standards can be used as transfer standards simulating up to 510 MBq when used in the UV-A and up to 8.7 GBq when used in the UV-C spectral regions.

## 2 Development of an alpha spectrometry source for traceable calibration of the radioluminescence detector systems

For traceable calibration of radioluminescence detector systems, it is necessary to use an alpha particle emitting source whose characteristics are traceable to national standards. The source should have as little angular dependence as possible, with the alpha particles emitted at their peak energy in a large solid angle close to  $2\pi$ . Since alpha particles in air must first generate radioluminescent light and this signal is then used to calibrate optical systems at some distance, the source of alpha radiation must be of appropriate strength to also achieve sufficient statistical uncertainty. Preliminary

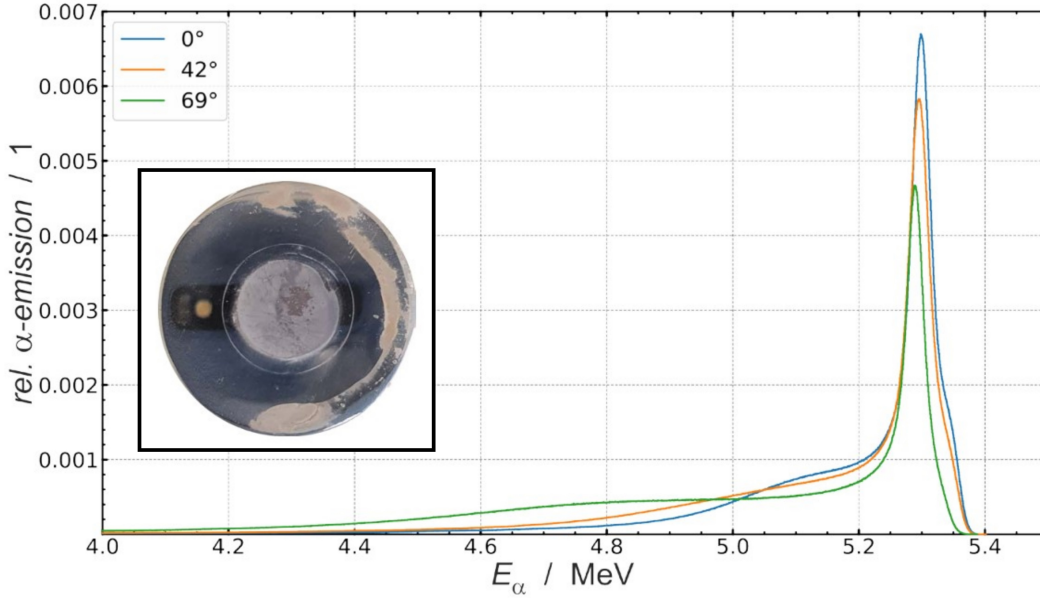


Figure 1: Relative alpha emission measured with a 25 mm<sup>2</sup> silicon surface barrier detector behind a 3.2 mm aperture and a distance from the source surface of 15 mm. The spectra have been measured at 0°, 42° and 69° relative to the surface normal. The inset shows the <sup>210</sup>Po sample with a diameter of 12 mm (central part) deposited on the silver substrate.

estimations based on tests with accelerated alpha particles at the PTB Ion Accelerator Facility indicated that an alpha activity between 500 kBq and 1 MBq would be well suited for calibration. The most widely used alpha spectrometry sources are made with <sup>241</sup>Am by electrodeposition from solution. However, since <sup>241</sup>Am has a long half-life with  $T_{1/2}^{\text{Am-241}} = 432.6(6)$  a [18], to achieve sufficient activity, a relatively large amount of mass must be deposited to the source, resulting in increased self-absorption. Additionally, since <sup>241</sup>Am has a relatively complex alpha spectrum with 5 transitions with probabilities above 0.1% between 5.38 MeV and 5.54 MeV, as well as a number of electron emissions and gamma transitions [18], a more suitable alternative, with higher specific activity, was explored.

This alternative is the <sup>210</sup>Po radionuclide. With a half-life of  $T_{1/2}^{\text{Po-210}} = 138.3763(17)$  d [18], the required film thickness is a factor of 1000 less than that of <sup>241</sup>Am for the same activity. Only 10 ng of <sup>210</sup>Po already correspond to an activity of 1.66 MBq. Moreover, <sup>210</sup>Po has only 2 alpha transitions, of which the higher energy one at 5.304 33(7) MeV has a transition probability of 99.998 76(4) % and a single gamma transition at 0.803 052(24) MeV which is practically negligible with a transition probability of only 0.001 23(4) %. Since <sup>210</sup>Po decays directly into the stable <sup>206</sup>Pb, no other radiation from the <sup>238</sup>U decay chain affects the measurement. Thus, the emission spectrum of a <sup>210</sup>Po source has the nearly ideal properties for traceable calibration of radioluminescence detector systems.

In this work, the <sup>210</sup>Po was dissolved out by dilute nitric acid from a composite containing silver and gold. Polonium is a relatively noble metal with a standard reduction potential of 0.8 V of the redox couple Po(IV)/Po(0). In aqueous solution, polonium exists hydrated as Po(IV) [19], and precipitates by reduction from aqueous or hydrochloric acid solutions on all metallic surfaces that are equally or less noble than silver, e.g., copper, nickel, and silver itself. This property does not apply to most other metals, so relatively pure polonium films can be obtained by electroless deposition. To prepare a source, the silver nitrate/polonium nitrate solution obtained was mixed with dilute hydrochloric acid (0.5 M HCl) and brought into contact with a polished sterling silver (925) target (30 mm diameter) at 50 °C. The target was mechanically polished to a mirror finish by using a polishing agent with an average grain size of 100 nm (Merard LUXOR orange). The area available for deposition was limited to a diameter of 12 mm by masking the rest of the target by polymethyl methacrylate (PMMA). The <sup>210</sup>Po source has been subsequently hardened at 250 °C.

A total of 840 kBq of <sup>210</sup>Po was deposited on the target and subsequently analyzed using the defined angle alpha spectrometry as the alpha-activity national standard [20]. The solid angle from the source to the detector is defined by an aperture system which is measured traceable to the national length. This defines the traceable solid angle and the PIPS detector has an efficiency of 1 for the alpha-particles in the regarded alpha-energy range [21]. A comparison of the

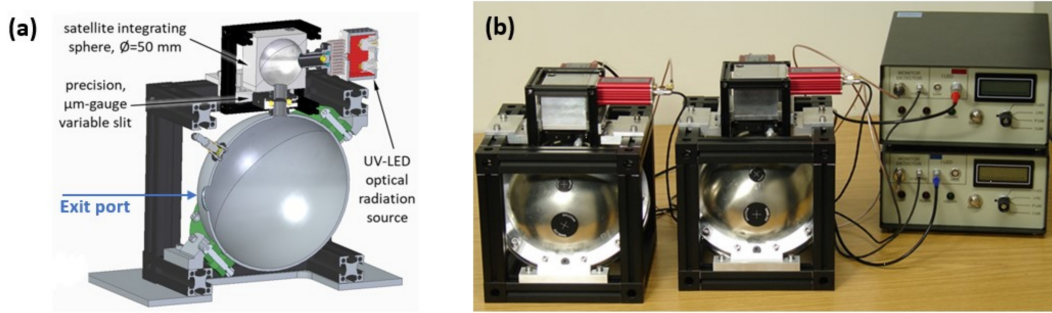


Figure 2: **(a)** Sectional schematic representation of the variable radiance, satellite integrating sphere-based configuration of the low photon flux UV radiance standard. **(b)** Realized prototypes of the variable low-photon flux UV-C (260 nm; left) and UV-A (340 nm; right) spectral range radiance standards for the calibration of the radioluminescence detector systems.

alpha spectra measured at different angles relative to the surface normal is shown in Fig. 1. Although some asymmetry in the measured spectra is still evident at low energies-mainly due to solution impurities deposited in the substrate-all spectra show a sharp peak at 5.30(1) MeV, with an FWHM of only 26.8(7) keV at 69° to 31.9(16) keV measured at 0° relative to the surface normal.

### 3 Novel low photon flux UV-radiance standards for the calibration of the radioluminescence detection systems

To implement the optical radiation calibration scheme, two new and dedicated variable low-photon flux, UV-C and UV-A radiance standards were designed, manufactured and radiometrically characterized. These radiation standards are portable and intended for use in the calibration of radioluminescence instruments without the need to relay in open alpha sources and stringent radiation protection protocols. Both radiance standards rely on integrating spheres as optical diffusors and share the same design concept (see Fig. 2):

- main integrating sphere diameter of 150 mm, radiating port of 25 mm diameter and two additional ports with 12.5 mm diameter,
- up to four orders of magnitude variable radiance via the application of a precision,  $\mu\text{m}$ -gauge variable slit and a satellite integrating sphere (50 mm diameter),
- aluminum spheres with high-purity alumina ( $\text{Al}_2\text{O}_3$ ) blasted, diffusely reflecting surface for enhanced stability in the UV spectral range,
- modular radiation sources port concept for UV-LED single/dual wavelength operation mode and additional continuum sources for spectral straylight simulation,
- monitor detector for radiance control and monitoring, and
- rigid aluminum rail framing for transportation and structural stability.

Radiance standards based on integrating spheres have the advantage that they represent a realization of a homogeneous Lambert radiator and are therefore a suitable transfer standard for the optical simulation of the radioluminescence radiation of an isotropic alpha particle radiator. UV LEDs with central wavelengths at 260 nm (UV-C; OPTAN-260J-BL) and 340 nm (UV-A; DUV340-HL18W), a spectral bandwidth (FWHM) of 11 nm and 8 nm, respectively, and an average radiant power of 1 mW are used as optical radiation sources. Their emission spectrum overlaps with the  $\text{N}_2$  + NO radioluminescence emission lines at 259.1 nm and the 337.1 nm line of  $\text{N}_2$ , respectively, which are selected by the interference filters for detection, allowing thus radiometric characterization of the radioluminescence detection systems in the respective spectral regions specified by their interference filters, see Fig. 3.

The low-photon flux radiance standards developed in the framework of RemoteALPHA were calibrated with the PTB transfer standards which consist of integrating sphere-based spectral radiance standards with 10 W tungsten halogen lamps as radiation sources, well characterized in terms of radiance stability and calibrated in terms of the absolute spectral radiance by direct comparison to the PTB primary radiance standard, the high-temperature blackbody HTBB3200pg at the PTB Spectral Radiance Comparator Facility [22]. Both low-photon flux radiance standards were

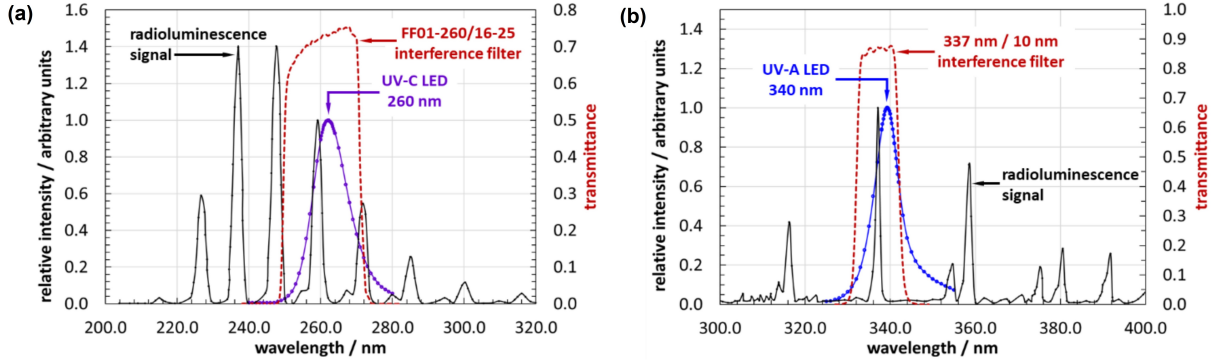


Figure 3: **(a)** UV-C radioluminescence spectrum of  $N_2+NO$  and 260 nm LED (OPTAN-260J-BL) emission spectra. **(b)** UV-A radioluminescence spectra of  $N_2$  and 340 nm LED (DUV340-HL18W) spectra. Also shown are the transmittances of the respective UV-C / UV-A interference filters. The UV-C radioluminescence spectrum data originate from [15], while the UV-A spectrum data from [1].

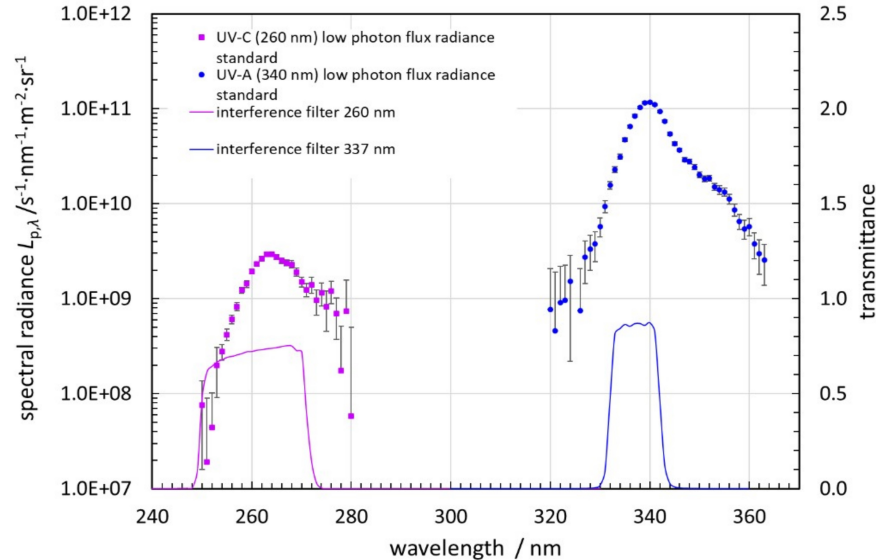


Figure 4: Calibrated spectral photon radiance of the UV-C / UV-A spectral range low-photon flux radiance standards (filled squares/circles). The uncertainty bars denote the type A standard uncertainty. Solid lines represent the manufacturer specified transmittances of the interference filters applied in the radioluminescence detectors.

calibrated with their variable slit setting fully open (7.5 mm) i.e., the setting with the maximum photon flux output [23]. The results for the calibrated spectral photon radiance of the UV-A and UV-C low-photon flux radiance standards are shown in Fig. 4.

The stability of the UV low photon flux radiance standards prototypes was examined for a period of 12 hours of continuous operation by measuring the output voltage of the monitor detectors. For the duration of the measurement, the radiance standards were installed inside a climatic chamber. A temperature cycle from  $19^\circ\text{C}$  to  $27^\circ\text{C}$  was conducted simultaneously to investigate the effect of environmental temperature change on the stability. Both radiance standards are stable within 0.1% for an observation period of 12 hours and an environmental temperature change of  $\pm 4^\circ\text{C}$ . The day-to-day variation lies within 0.03%. If a warming-up time of approximately 1 hour is respected, the stability is within 0.02% [23].

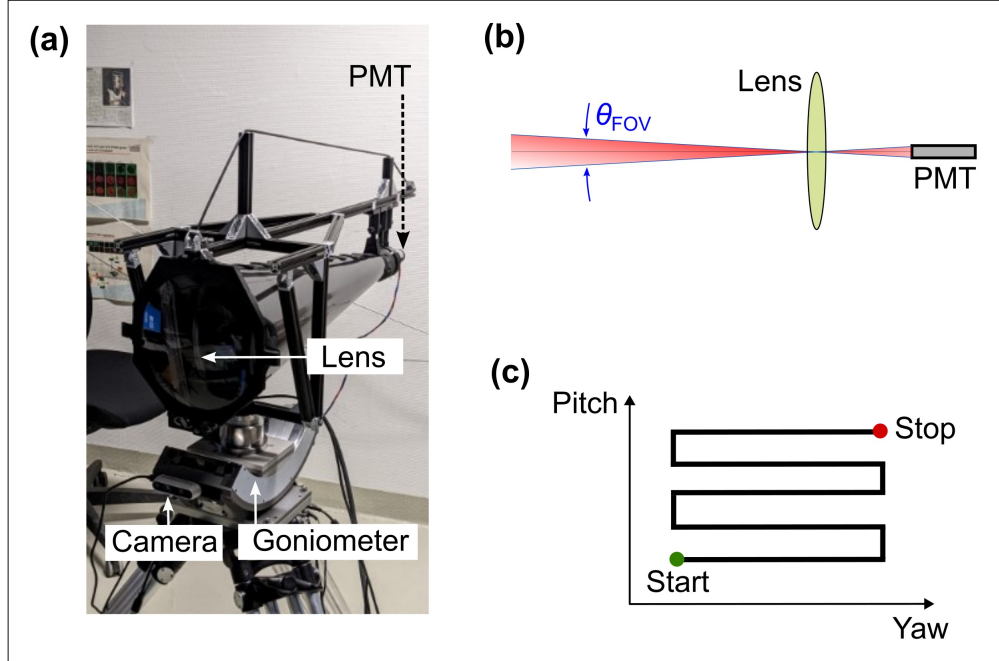


Figure 5: **(a)** The UVFS lens radioluminescence detection system developed in the framework of RemoteALPHA. By using the appropriate interference filters and PMTs, it can operate in both UV-A and UV-C spectral regions, respectively. The system also features a two-stage goniometer and an Intel RealSense D435 depth camera which takes an RGB color image and appends it with the depth information allowing superimposing the ultraviolet scan onto the RGBD image. **(b)** Schematic illustration of the field-of-view (FOV) quantified with the angle of view  $\theta_{\text{FOV}}$  in a radioluminescence detection setup composed of a lens and a photomultiplier (PMT). **(c)** Schematic illustration of the serpentine scanning applied to map the scene.

#### 4 Detection system and the experimental setup

In the framework of RemoteALPHA, telescopes based on fused silica and Poly(methyl 2-methylpropenoate) (PMMA) Fresnel lenses have been developed and investigated for their usability in facilitating emergency management related to alpha-emitting radionuclides [17, 24]. These systems were designed from the outset to facilitate emergency management by maximizing radioluminescence throughput through large receiving optics and keeping the background signal low through efficient wavelength filtering and low-noise photomultipliers (PMTs). Due to the superior transmission properties in the entire UV spectral range (UV-A to UV-C) of fused silica compared to PMMA, the radioluminescence detection system based on a fused silica lens has been adopted as a transfer instrument to establish a traceable relationship between the activity and the radioluminescence flux in the spectral range of interest.

This reference instrument consists of a 240 mm diameter planoconvex UV- grade Fused Silica (UVFS) lens (Abet Technologies), a filter set to select the operating wavelength range (UV-A or UV-C), and a PMT with a cathode material corresponding to the wavelength range selected by the filter set:

- in UV-A, a bialkali photocathode PMT (H10682-210, Hamamatsu) is used with a 2-filter assembly consisting of Edmund Optics #65-189 and Semrock FF01-340/12-25 centered at 337 nm and 340 nm, respectively, and
- in UV-C, a cesium telluride photocathode PMT (H11870-09, Hamamatsu) is used with one or, when specified, two Semrock FF01-260/16-25 filter centered at 260 nm.

The entire optical system is contained in an aluminum frame mounted on a motorized tilt and yaw platform consisting of a goniometer and rotary stage (Newport MBGM160PE and RVS80CC), see Fig. 5. The UVFS lens radioluminescence detection system (Fig. 5(a)) operates as scanning system by producing the radioluminescence image of the alpha-emitting sources through remote scanning of narrow FOV ( $\theta_{\text{FOV}}$  of about  $1^\circ$ ) over the user-defined region of interest while recording the photon count rate (Fig. 5(b)). Scanning is performed in a serpentine pattern from the lower left corner (Fig. 5(c)), traversing the entire yaw area at each pitch step. The scanning speed is typically set to  $10^\circ \text{s}^{-1}$  and  $0.5^\circ \text{s}^{-1}$  for the yaw and pitch steps, respectively. Unlike an imaging system, which requires additional optical

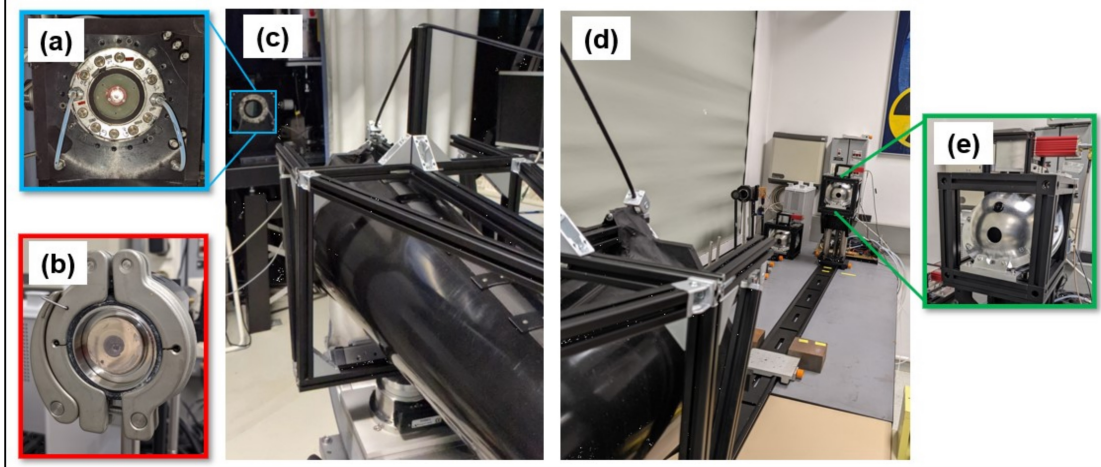


Figure 6: Experimental setup used for the calibration of the UVFS lens radioluminescence setup with the  $^{210}\text{Po}$  activity standard and for cross-calibration of UV-A and UV-C radiation standards. (a)  $^{210}\text{Po}$  activity standard in the experimental chamber with quartz window that can be filled with different gases (air,  $\text{N}_2$ ,  $\text{N}_2+\text{NO}$  mixture). (b)  $^{210}\text{Po}$  activity standard mounted in a KF25 wing nut clamp set for use in air for cross-calibration of UV-C and UV-A radiation standards. (c) Photo of the experimental setup during calibration of the UVFS lens detection setup with  $^{210}\text{Po}$  activity standard. (d) Photo of the experimental setup during cross-calibration of the UV radiation standards with the UVFS lens system. (e) Photo of the UV-C radiation standard.

elements to correct for image distortion and aberration, the UVFS lens scanning system was designed for a minimal number of refractive elements to reduce unnecessary light loss. In addition, more than one interference filter can be used without having to account for distortions caused by multiple reflecting surfaces. For sensitivity studies, the  $^{210}\text{Po}$  activity standard is mounted in an evacuable experimental chamber with a quartz window (Fig. 6 (a)). This allows the space around the source to be filled with selected gases and the radioluminescence outside the chamber to be studied in the relevant wavelength range. When calibrating the radiation standard, the source was mounted in a wing nut clamp for KF25 flanges (Fig. 6(b)) so that it could be integrated into the same setup as the UV-A and UV-C radiation standards and measured sequentially with them (Fig. 6 (d,e)). In all cases, the optical detection systems were set up at a distance of 2 m from the source.

## 5 Experiment results and discussion

Figure 7 shows the UV-A radioluminescence image of the  $^{210}\text{Po}$  activity standard in air (i.e., the experimental chamber was filled with air at atmospheric pressure) measured with the UVFS lens radioluminescence detection system at a distance of 2 m. The source was mapped over an angular range of  $2.5^\circ$  in both tilt and rotation, with an angular resolution of  $0.05^\circ$  and a PMT integration time of 1 s per measurement point. The left panel shows the UV-A radioluminescence image superimposed on a conventional photograph of the scene taken by the Intel RealSense D435 depth camera integrated into the detection system, while the right panel shows the 2D distribution of the UVC radioluminescence signal in the image plane. Since the field of view of the detection system (about  $1^\circ$ ) is larger than the angular resolution of the scan, the radioluminescence image is comprised of overlapping fields of view between adjacent scan points, resulting in a convolution of the true radioluminescence image with the point spread function (PSF) of the detection system. Since PSF is susceptible to motion blur and is not error-free, each deconvolution step will introduce inaccuracies in the deconvoluted image which will propagate further to the detector sensitivity quantification. To avoid these problems, the sensitivity of the detection system was determined using a method proposed by Luchkov et al. [25], in which the relationship between the net radioluminescence intensity and the source activity is derived from the 2D integral of the net count rate per pixel over the source area. This yields the following equation for the sensitivity:

$$S = \frac{R^2 \sum_{\text{net}}}{T A_s} \quad (1)$$

where  $\sum_{\text{net}}$  is the sum of the net count rate (gross signal minus background) per pixel in the source region (region with a pixel count rate greater than the average background count rate),  $A_s$  is the activity of the sample,  $T$  is the transmittance of the quartz window, and  $R$  is the dimensionless scan resolution ( $R = \Delta\theta/1^\circ = \Delta\psi/1^\circ$  with  $\Delta\theta$  and  $\Delta\psi$  being

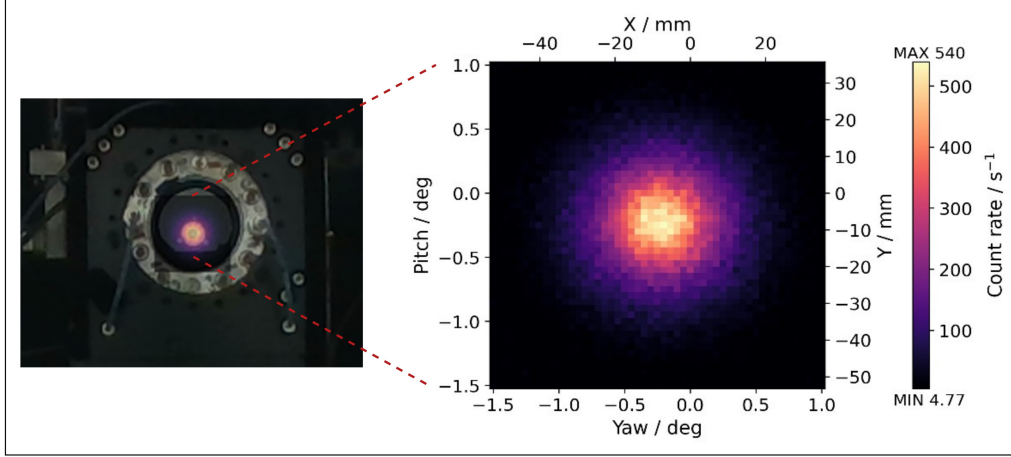


Figure 7: UV-A radioluminescence image of a  $^{210}\text{Po}$  activity standard in the experimental chamber filled with air at atmospheric pressure.

Table 1: Sensitivity of the UVFS lens detection system measured with the  $^{210}\text{Po}$  activity standard. All uncertainties reported in the table (and those throughout the text) have a level of confidence of approximately 68% (coverage factor  $k = 1$ ).

Spectral range	Atmosphere	Sensitivity ( $\text{s}^{-1} \text{MBq}^{-1}$ )
UV-A	Air	662(44)
UV-A	$\text{N}_2$ atmosphere	5587(370)
UV-A	$\text{N}_2+\text{NO}$ atmosphere	7450(494)
UV-C	Air	34.1(24)
UV-C	$\text{N}_2$ atmosphere	2533(168)
UV-C	$\text{N}_2+\text{NO}$ atmosphere	181 960(12056)

the scan resolution in degree in pitch and yaw, respectively). For the radioluminescence image in Fig. 7 (left panel), with  $R = 0.05$ ,  $A_s = 0.648(41) \text{ MBq}$ ,  $T = 0.91(2)$  and  $\sum_{\text{net}} = 156\,214(442) \text{ s}^{-1}$ , a sensitivity  $S = 662(44) \text{ s}^{-1} \text{MBq}^{-1}$  is obtained. The uncertainty of the sensitivity is influenced largely by the uncertainty of the  $^{210}\text{Po}$  source. This was estimated by propagating the uncertainties  $u(\sum_{\text{net}})$ ,  $u(A_s)$  and  $u(T)$  into the sensitivity equation (1).

Figure 8 compares the UV-C radioluminescence images of the  $^{210}\text{Po}$  activity standard measured in air (a),  $\text{N}_2$  atmosphere (b), and in the  $\text{N}_2+\text{NO}$  atmosphere (c). The results of sensitivity measurements in UV-A and UV-C spectral regions at different atmospheres are summarized in Table 1. The UV-A sensitivity measured in air compares well with the value measured with reference sources of  $^{239}\text{Pu}$ ,  $760(100) \text{ s}^{-1} \text{MBq}^{-1}$ , under similar experimental conditions [25]. In the  $\text{N}_2$  atmosphere, the sensitivity is increased by factor of 8, which is due to the removal of quenchers such as oxygen and humidity from the chamber. This increase compares well with the factor 6 increase reported in [3] and factor of 10 in [2], with the difference predominantly due to the remaining impurities in the experimental chamber, verified quantitatively by varying the  $\text{N}_2$  flow rate. The use of  $\text{N}_2 + \text{NO}$  mixture led to about 25% increase of the sensitivity relative to  $\text{N}_2$ . The effect of  $\text{N}_2+\text{NO}$  purging is especially apparent in case of UV-C spectral region (see [11, 15, 17]). Here we observe an increase of sensitivity by three orders of magnitude relative to the air measurements, of the same order of magnitude as the increase observed in [17]. The increase of the signal in the  $\text{N}_2+\text{NO}$  mixture is due to excitation transfer from  $\text{N}_2$  to  $\text{NO}$  [15], which is less prone to quenching relative to  $\text{N}_2$ . The increase of UV-C sensitivity in  $\text{N}_2$  atmosphere relative to air is mainly related to trace amounts of  $\text{NO}$  in the  $\text{N}_2$  and the removal of quenching gases.

Featuring a high specific activity and a sharp alpha peak, the  $^{210}\text{Po}$  source has nearly ideal properties for traceable calibration of radioluminescence detector systems. The main drawback of using  $^{210}\text{Po}$  for routine calibrations is its short half-life of  $138.3763(17) \text{ d}$ , which requires relatively high activity when such a source is provided as a long-term calibration service. In addition, these services involve rigorous radiation protection measures and high operational costs. These disadvantages can be overcome if the calibration of novel radioluminescence systems is based on all-optical radiation devices as transfer standard sources instead.

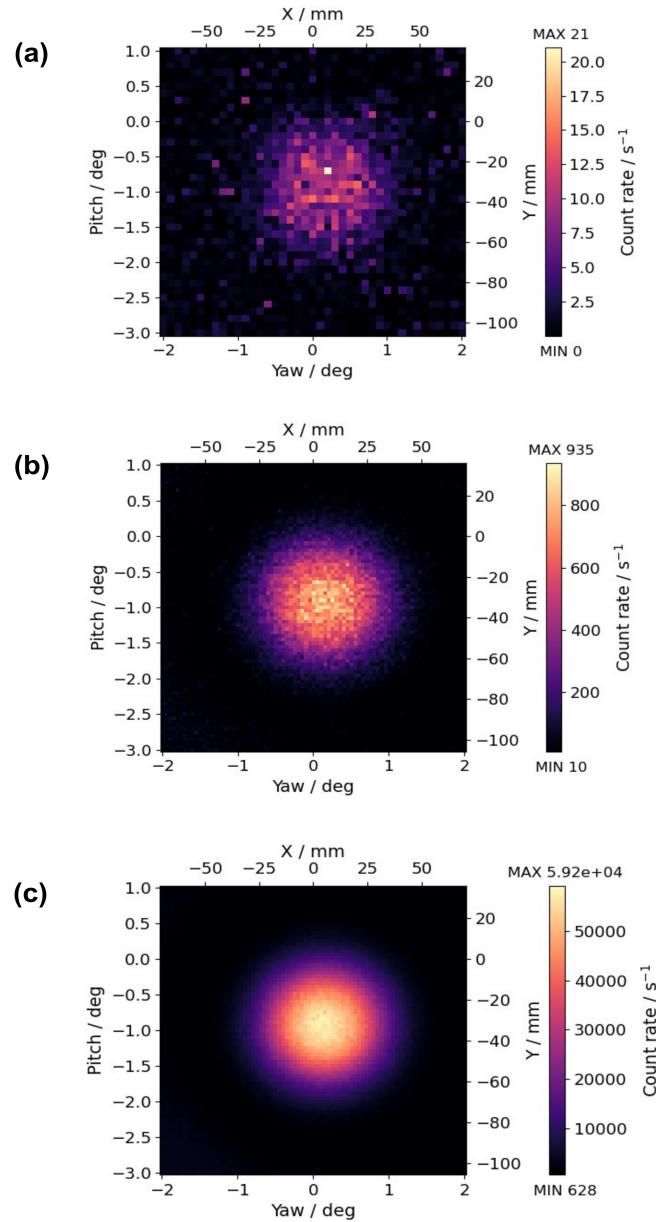


Figure 8: UV-C radioluminescence images of  $^{210}\text{Po}$  in (a) air, (b)  $\text{N}_2$  atmosphere ( $\text{N}_2$  flow rate: 5 L/min), and (c)  $\text{N}_2+\text{NO}$  atmosphere ( $\text{N}_2 + \text{NO}$  flow rate: 0.95 L/min, with 10 ppm NO). For all measurements, the Hamamatsu PMT with CsTe photocathode (H11870-09) was used with a single bandpass interference filter having a bandwidth of 16 nm and center wavelength of 260 nm (FF01-260/16–25, Semrock Inc.).

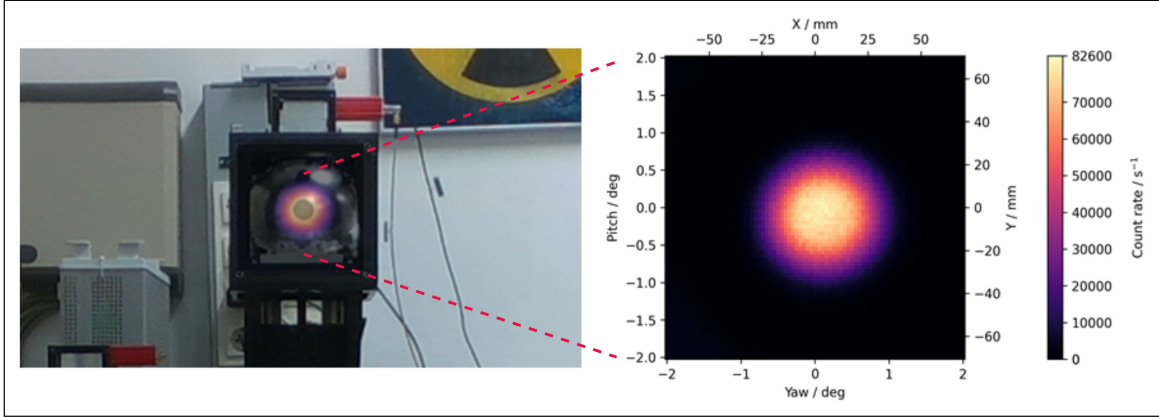


Figure 9: Mapping of simulated radioluminescence by the low-photon flux radiance standard at 260 nm measured by the UVFS detection system. The left panel shows the overlay of the UV-C signal distribution with the image of the radiance standard. The right panel shows the UV-C signal measured using two Semrock FF01-260/16-25 filters.

To implement the optical radiation calibration scheme, as a mandatory prerequisite, a traceable relationship between radiometric quantities (e.g., photon flux rate) and activity must be established. In this work, the radiance standards were (a) radiometrically characterized and calibrated with a PTB primary radiation standard (a high-temperature blackbody radiator HTBB3200pg), and (b) were cross-calibrated in terms of the activity using the UVFS lens system as an intermediate activity transfer standard.

Cross-calibration of the low flux UV-A and UV-C radiation standards was performed by comparing their spectral radiance with the radioluminescence signal in the respective UV wavelength bands. All measurements were performed consecutively on the same day in the laboratory at an air temperature of  $T = 21(1)^\circ\text{C}$ , a humidity  $H$  between 30% and 50%, and an atmospheric pressure of  $P = 1005(13)$  hPa. The optical axis of the optical detection system was aligned using a 2D scan similar to those shown in Figs. 7 and 9. All radiation sources were positioned 2 m from the lens of the UVFS lens system and aligned so that their centers were on the optical axis of the detection system. The signal from the radiation standards was then mapped to activity using the radioluminescence signal from  $^{210}\text{Po}$  as a reference value and accounting for the detector's linearity. For both wavelength ranges (UV-A at 340 nm and UV-C at 260 nm), the photon flux from the radiation standards does not saturate the radioluminescence detector at the highest setting, i.e., with the variable slit fully open, and the linearity of the UVFS lens detection system is maintained over the entire measurement range.

Varying the slit width from 0.02 mm to 7.5 mm (fully open), alpha sources with activities from  $5.8 \times 10^4$  Bq to  $8.3 \times 10^8$  Bq can be simulated with the 340 nm UV-A radiance standard and from  $2.9 \times 10^5$  Bq to  $5.7 \times 10^9$  Bq with the 260 nm UV-C radiance standard (see Fig. 10). The differences in the highest simulated activity or highest radiance are due to the different power output of the LEDs used. The dependence of the integrated photon radiance with the activity is shown in Fig. 10 (b,d). As expected, the photon flux exhibits linear dependence on the activity. The dependence on the slit width, on the other hand is quadratic (Fig.10 (a,c)), proportional to the integrating spheres junction area controlled by the slit (cf. Fig. 2). As the  $^{210}\text{Po}$  activity was around 175(11) kBq at the time of calibration of radiance standards, counting statistics during the  $^{210}\text{Po}$  radioluminescence measurement account for the majority of uncertainties in Fig. 10. The relative standard uncertainty ( $k = 1$ ) of the integrated photon flux at the highest setting (fully opened slit) is estimated to 8 % for the 260 nm UV-C radiance standard resp. 4 % for the 340 nm UV-A radiance standard. The main contribution to the uncertainty budget arises from photon counting statistics, followed by the uncertainty contribution from the transfer radiance standard applied for calibration.

The presented spectral radiance to activity relationship only exists in defined wavelength bands specified by the band-pass of the interference filters used in the transfer instrument (i.e., UVFS lens detection system) since the emission spectrum of the LEDs built into the radiant standard does not exactly match the real radioluminescence spectrum of air (nitrogen). The wavelength bands are defined as follows: 260 nm central wavelength with 16 nm bandwidth for UV-C, and 340 nm central wavelength with 12 nm bandwidth for UV-A range. The use of different filter configurations (central wavelength, bandwidth) including the filter-free setup would require a reconfiguration of the low-photon flux radiance standards with respect to the used optical radiation sources for a wavelength range match to the detector system and a subsequent recalibration of the radiance standards. These state-of-the-art portable calibration standards are critical to ensure the quality of measurements made with radioluminescence detection systems through regular

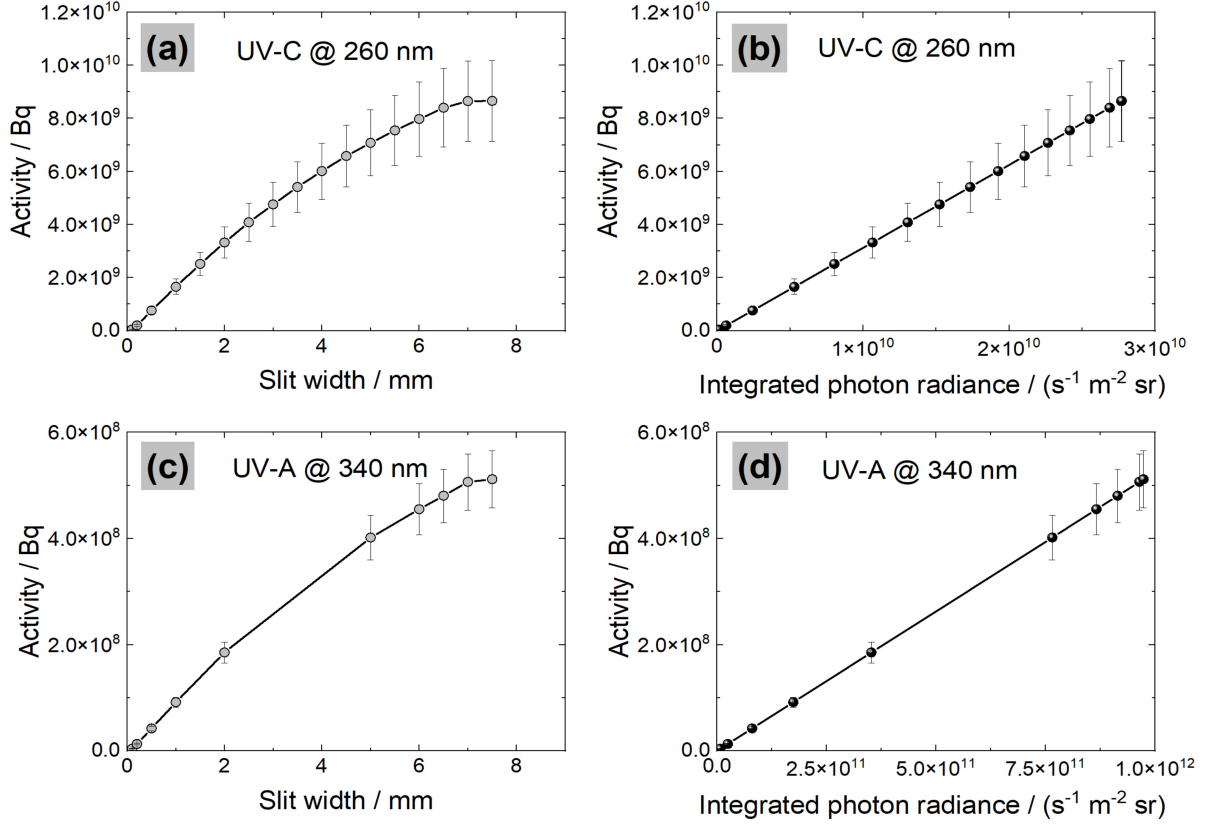


Figure 10: The relationship between slit width and integrated photon radiance of radiance standards to activity. Panels (a) and (b) correspond to the UV-C radiance standard while (c) and (d) to the UV-A radiance standard. The integrated spectral radiance wavelength range is from 252 nm to 268 nm in UV-C and from 334 nm to 346 nm in UV-A.

calibration both before and after the equipment is used. They also play an important role in the design and optimization of radioluminescence setups, e.g., in the optimization of lens or mirror configurations, but also in the optimization of filter setups, since the angle between filters is crucial to avoid getting a Fabry-Perot interferometer-like system which deteriorates the radioluminescence signal.

## 6 Conclusion

Sound interpretation and, in particular, comparability of radioluminescence measurement data can only be ensured if the measurement equipment used for this purpose is traceable to the SI system of units. Two complementary metrological approaches were developed to facilitate the deployment of novel-type alpha-radioluminescence detection systems to radiological emergency management, nuclear safeguards, nuclear decommissioning, and nuclear forensics. The first method is based on a dedicated <sup>210</sup>Po activity standard which is used to determine the sensitivity of the radioluminescence detection setup and thus to establish a traceable relationship between the alpha activity and radioluminescence intensity. The <sup>210</sup>Po radionuclide was selected as a perfect candidate for the alpha activity standard due to its well-defined alpha energy (single  $\alpha$ -emission,  $E_\alpha = 5.304\,33(7)$  MeV, with an emission probability  $p_\alpha = 99.99876\%$ ) and virtually no gamma radiation (the emission probability for gamma emission at  $E_\gamma = 803.052(24)$  keV is only 0.001 23(4) %). The source was prepared from the silver nitrate/polonium nitrate solution mixed with dilute hydrochloric acid (0.5 M HCl) and was deposited in on a silver substrate with an active area having a diameter of 12 mm. The source was characterized in a Defined Solid Angle  $\alpha$ -Spectrometer where the alpha spectrum has been measured. The source has a peak at about 5.3 MeV with energy spread (FWHM) of only 26.8(7) keV at 69° to 31.9(16) keV measured at 0° relative to the surface normal.

Since <sup>210</sup>Po has a short half-life of 138.4 d, either a relatively high activity must be deposited if such a source is offered as a long-term calibration service, or it must be replaced frequently. Therefore, the use of this approach for routine

calibrations and/or in-field measurements, but also more generally for quality assurance purposes, is a challenging task with significant potential for radiological accidents that might occur during the fabrication, handling, and storage of such an activity standard. This requires stringent radiation protection measures in management and monitoring of such activity standards, as well as high maintenance costs. To overcome these difficulties, the second approach based on all-optical calibration sources has been developed. Two radiation standards to simulate alpha radioluminescence in the UV-A and UV-C spectral regions have been developed. Both radiation standards are based on two interconnected integrating spheres and mimic a planar alpha radiation sample with a diameter of 25 mm with a predefined activity. They have isotropic optical emission properties with a Lambertian distribution of radiance within  $\pm 6$  degree of the normal to the radiation surface. Their spectral photon radiance is traceable to the PTB primary radiance standard, the high-temperature blackbody HTBB3200pg. They were cross-calibrated for activity using the UVFS lens system, which serves as a transfer instrument. By varying the slit width from 0.02 mm to 7.5 mm (fully open), an alpha source activity of  $3.6 \times 10^4$  Bq to  $5.1 \times 10^8$  Bq can be simulated with the UV-A standard at 340 nm and of  $4.4 \times 10^5$  Bq to  $8.7 \times 10^9$  Bq with the UV-C standard at 260 nm.

The calibration methodologies presented in this paper are essential for a rapid and appropriate response by nuclear regulatory authorities and other decision-makers (e.g., local authorities or response organizations) both during and in the aftermath of a nuclear or radiological accident. They help provide reliable radiological data that enable appropriate countermeasures and reduce the risk of overreaction and avoidable follow-up costs. Ensuring that novel radioluminescence detection systems correctly quantify the measured radioluminescence signal is also critical for crime scene investigation (including illicit trafficking of alpha emitters), but also benefits the nuclear industry during decommissioning operations.

## Acknowledgement

This project 19ENV02 RemoteALPHA has received funding from the EMPIR programme co-financed by the Participating States and from the European Union's Horizon 2020 research and innovation programme. 19ENV02 RemoteALPHA denotes the EMPIR project reference.

## References

- [1] S. M. Baschenko. Remote optical detection of alpha particle sources. *J. Radiol. Prot.*, 24:75, 2004.
- [2] J. Sand. *Alpha Radiation Detection via Radioluminescence of Air*. PhD thesis, Tampere University of Technology, Tampere, Finland, 2016. Publication; Vol. 1449.
- [3] J. Sand, S. Ihtola, K. Peräjärvi, H. Toivonen, and J. Toivonen. Radioluminescence yield of alpha particles in air. *New Journal of Physics*, 16:053022, 2014.
- [4] W Huggins and L. Huggins. On the spectrum of the spontaneous luminous radiation of radium at ordinary temperatures. *Proceedings of the Royal Society of London*, 72:196, 1903.
- [5] W Huggins and L. Huggins. On the spectrum of the spontaneous luminous radiation of radium. Part III. Radiation in hydrogen. *Proceedings of the Royal Society of London*, 76:488, 1905.
- [6] W Huggins and L. Huggins. On the spectrum of the spontaneous luminous radiation of radium. Part IV. Extension of the glow. *Proceedings of the Royal Society of London Series A*, 77:130, 1906.
- [7] T. Waldenmaier. *Spectral resolved measurement of the nitrogen fluorescence yield in air induced by electrons*. PhD thesis, Forschungszentrum Karlsruhe in der Helmholtz-Gemeinschaft, Karlsruhe, Germany, 2006. Wissenschaftliche Berichte FZKA 7209.
- [8] F. Kakimoto, E. C. Loh, M. Nagano, M. Okuno, M. Teshima, and S. Ueno. A measurement of the air fluorescence yield. *Nuclear Instruments and Methods in Physics Research Section A*, 372:527, 1996.
- [9] J. Rosado, F. Blanco, and F. Arqueros. Comparison of available measurements of the absolute air-fluorescence yield. *Astroparticle Physics*, 34:164, 2010.
- [10] F. Lamadie, F. Delmas, C. Mahe, P. Gironès, C. Le Goaller, and J. R. Costes. Remote alpha imaging in nuclear installations: New results and prospects. *IEEE Transactions on Nucl. Sci.*, 52:3035, 2005.
- [11] F. S. Krasniqi, T. Kerst, M. Leino, J.-T. Eiseh, H. Toivonen, A. Röttger, and J. Toivonen. Imaging of alpha emitters in a field environment. *Nuclear Instruments and Methods in Physics Research Section A*, 987:164821, 2021.
- [12] S. Yamamoto and H. Tomita. Comparison of light outputs, decay times, and imaging performance of a ZnS(Ag) scintillator for alpha particles, beta particles, and gamma photons. *Appl Radiat Isot.*, 168:109527, 2021.

- [13] T. H. N Phong, T. N. Van, and H. L. Cong. Efficiency response of an aged PIPS detector used in high-resolution alpha-particle spectrometry. *Nuclear Instruments and Methods in Physics Research Section A: Accelerators, Spectrometers, Detectors and Associated Equipment*, 908:128, 2018.
- [14] J.E. Noakes and J.L. Duggan. A high resolution  $4\pi$  alpha spectrometer with silicon surface barrier detectors. *J. Radioanal. Chem.*, 43:399, 1978.
- [15] T. Kerst and J. Toivonen. Intense radioluminescence of NO/N<sub>2</sub>-mixture in solar blind spectral region. *Optics Express*, 26:33764, 2018.
- [16] EURAMET, 19ENV02 RemoteALPHA. Remote and real-time optical detection of alpha-emitting radionuclides in the environment. <https://www.euramet.org/research-innovation/search-research-projects/details/project/remote-and-real-time-optical-detection-of-alpha-emitting-radionuclides-in-the-environment/>. Accessed: 2023-10-25.
- [17] M. Luchkov, V. Dangendorf, U. Giesen, F. Langner, C. Olaru, M. Zadehraf, A. Klose, K. Kalmankoski, J. Sand, S. Ihantola, H. Toivonen, C. Walther, S. Röttger, M.-R. Ioan, J. Toivonen, and F. S. Krasniqi. Novel optical technologies for emergency preparedness and response: Mapping contaminations with alpha-emitting radionuclides. *Nuclear Instruments and Methods in Physics Research Section A: Accelerators, Spectrometers, Detectors and Associated Equipment*, 1047:167895, 2023.
- [18] X. Mougeot et al. The Decay Data Evaluation Project (DDEP), Atomic and Nuclear data. <http://www.lnhb.fr/nuclear-data/nuclear-data-table>. Accessed: 2023-08-27.
- [19] Figgins, P. E. *The Radiochemistry of Polonium*. National Academy of Sciences, 1961.
- [20] To be published elsewhere.
- [21] Pommé. The uncertainty of counting at a defined solid angle. *Metrologia*, 52:73, 2015.
- [22] R. Friedrich and J. Fischer. New spectral radiance scale from 220 nm to 2500 nm. *Metrologia*, 37:539, 2000.
- [23] R. D. Taubert, M. Luchkov, P. Gál, M.-R. Ioan, and F. Krasniqi. Design and Characterisation of a Low-Photon Flux UV-Radiance Standard for the Calibration of Radioluminescence Detection Systems. Submitted to: Journal of Physics: Conference Series, 15th International Conference on New Developments and Applications in Optical Radiometry (NEWRAD 2023).
- [24] A. Klose, M. Luchkov, V. Dangendorf, A. Lehnert, and C. Walther. On the way to remote sensing of alpha radiation: radioluminescence of pitchblende samples. Submitted to Journal of Radioanalytical and Nuclear Chemistry.
- [25] M. Luchkov, C. Olaru, I. Lalau, M. Zadehraf, I. R. Nikolényi, Z. Gémesi, M. R. Ioan, and F. Krasniqi. Radioluminescence mapping of <sup>241</sup>Am-doped environmental samples and nuclear materials. Journal of Radioanalytical and Nuclear Chemistry (Accepted).